J. Biochem. 2009;146(3)359–368
doi:10.1093/jb/mvp078

Domain-dependent Interaction of Eukaryotic Initiation Factor eIF4A for Binding to Middle and C-terminal Domains of eIF4G

Yuki Fujita[1], Masako Oe[1], Tatsuya Tutsumino[1], Shigenobu Morino[1,*], Hiroaki Imataka[2], Koji Tomoo[1,†] and Toshimasa Ishida[1]

[1]Department of Physical Chemistry, Osaka University of Pharmaceutical Sciences, 4-20-1 Nasahara, Takatsuki, Osaka 569-1094, Japan; and [2]Riken Genomic Sciences Center, 1-7-22 Suehiro-cho, Tsurumi-ku, Yokohama City, Kanagawa, 230-0045, Japan

Received April 28, 2009; accepted May 11, 2009; published online May 26, 2009

The interactions of recombinant human eIF4A (4A) and its N- and C-terminal side domains (AN and AC, respectively) with the middle- and C-terminal-domain-linked fragment (GMC) of eIF4G and its middle and C-terminal domains (GM and GC, respectively) were investigated by surface plasmon resonance (SPR) analysis and isothermal titration calorimetry (ITC). It is remarkable that the kinetic parameter-dependent SPR profile observed for the 4A–GMC pair was quite different from the steady affinity profiles of the 4A–GM/GC pairs, suggesting the simultaneous contribution of the middle and C-terminal domains of eIF4G for the binding with eIF4A. On the other hand, ITC yielded the enthalpy energies of -1.5×10^4 to -2.5×10^4 J/mol for the domain–domain interactions of 4A with GMC. Although the ITC profile of the 4A–GM pair reflects well the structural feature shown previously by NMR and X-ray analyses, it was essentially different from that of the 4A-GMC pair. The present results suggest that the intimate interaction between the eIF4A N- and C-terminal domains and the eIF4G middle and C-terminal domains is necessary to reveal the biologically active function of the eIF4A–eIF4G complex.

Key words: eIF4A, eIF4G, association, domain–domain interaction, surface plasmon resonance, isothermal titration calorimetry.

Abbreviations: 4A, eukaryotic initiation factor 4A; AN, eIF4A N-terminal domain; AC, eIF4A C-terminal domain; GM, eIF4G middle domain; GC, eIF4G C-terminal domain; GMC, middle- and C-terminal-domain-linked fragment of eIF4G; GST, glutathione S-transferase; CD, circular dichroism; CM5, carboxymethylated dextran; eIF4A, eukaryotic initiation factor 4A; eIF4E, eukaryotic initiation factor 4E; eIF4G, eukaryotic initiation factor 4G; HEPES, 2-(4-(2-hydroxyethyl)-1-piperazinyl)ethanesulfonic acid; IPTG, isopropyl-β-D-thio-galacto- pyranoside; ITC, isothermal titration calorimetry; mRNA, messenger RNA; NTA; nitrilotriacetic acid; PABP, poly(A)-binding protein; PCR, polymerase chain reaction; SPR, surface plasmon resonance.

Most eukaryotic mRNAs have a cap structure (m^7GpppN, where N is any nucleotide) at their 5′ end and a poly(A) tail structure at their 3′ end. One of the most highly regulated steps in translation initiation is mRNA recruitment, which requires the recognition of the 5′-terminal cap and 3′-terminal poly(A) tract, the unwinding of the 5′-terminal secondary structure and binding to the 43 S initiation complex (*1–3*). These steps are mainly mediated by the initiation factors of the eIF4 group (eIF4F and eIF4B) and poly(A)-binding protein (PABP) (*4*). The eukaryotic initiation factor 4F (eIF4F) is a supramolecular complex consisting of three subunits, eIF4E, eIF4A and eIF4G, and catalyses the initiation of cap-dependent translation with a sequential function.

eIF4E participates in the first step of the translation initiation through the direct recognition of the mRNA cap structure. eIF4A is a member of the DEAD/H-box RNA helicase family, a diverse group of proteins that couple ATP hydrolysis to RNA binding and duplex separation and melts the secondary structure of the mRNA 5′-untranslated region to facilitate ribosome binding (*5*, *6*). eIF4G is an adaptor protein with a modular structure and serves as a scaffold for eIF4E, PABP and eIF4A to coordinate their functions, thus playing a key function in translation initiation (*4*, *7–9*).

The binding sites of these initiation factors in the sequence of human eIF4G are shown in Fig. 1. The N-terminal one-third (amino acids 1–634) of eIF4G contains eIF4E and PABP binding sites (*10–12*), the middle third (amino acids 635–1039) possesses eIF3 and eIF4A binding sites as well as an RNA binding site (*13*, *14*), and the C-terminal one-third (amino acids 1040–1600) carries a second binding site for eIF4A and a binding site for the protein kinase Mnk1, which phosphorylates eIF4E (*13–15*). Analyses of the relationships of eIF4G with these initiation factors are important in understanding the structure–function relationships of these initiation factors in the initiation phase of cap-dependent translation.

*Present address: Screening Science, Lead Discovery Research Labs. Drug Discovery Research, Astellas Pharma Inc. 21, Miyukigaoka, Tsukuba-shi, Ibaraki 305-8585, Japan.
†To whom correspondence should be addressed.
Tel: +81-72-690-1069, Fax: +81-72-690-1068,
E-mail: tomoo@gly.oups.ac.jp

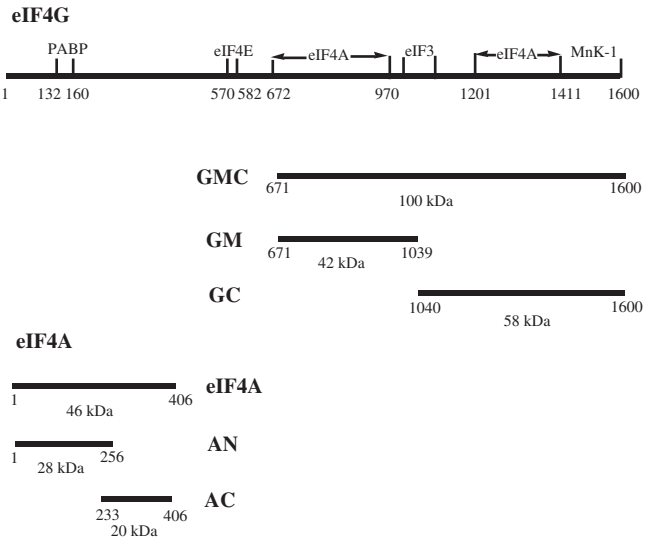

Fig. 1. **Binding sites of initiation factors on eIF4G and recombinant human eIF4G and eIF4A fragments used in this study.** The amino-acid residues present in each fragment and the molecular mass are indicated below the bar.

Concerning the interaction between eIF4A and eIF4G, Morino *et al*. (*9*) reported that the interaction of the eIF4G middle region with eIF4A is necessary for translation and that the C-terminal region serves as a modulator. To understand how eIF4G enhances the RNA helicase activity of eIF4A, structural and spectroscopic studies have been performed to model a binding architecture (*16–24*). The crystal structure of yeast eIF4A showed a dumbbell structure of two compact N- and C-terminal domains connected by an extended linker (*25–27*), and the crystal structures of the middle (*18*) and C-terminal (*19*) domains of eIF4G showed the eIF4A-binding regions consisting of helices arranged as HEAT repeats. Also, a binding model of eIF4A with the middle domain of eIF4G, analyzed by NMR chemical shift mapping and site-directed mutagenesis (*23*) and by X-ray crystal structure (*24*), showed that the structural scaffold of eIF4G middle domain is a soft clamp for stabilizing the active conformation of eIF4A. Nevertheless, the models proposed thus far do not satisfactorily explain why eIF4G requires two different eIF4A binding sites and how it enhances the ATP-stimulated helicase activity of eIF4A. This is primarily due to the lack of the systematic analysis on the whole interaction feature of the eIF4A–eIF4G complex, in which all the domains necessary for the interaction of both molecules are included.

To understand the intact interaction between eIF4G and eIF4A, it is important to examine how and to what extent the middle and C-terminal domains of eIF4G contribute to the binding with the N- and C-terminal domains of eIF4A, because no systematic study of the separated and linked domain–domain interactions between both proteins has been reported yet. Thus, we prepared recombinant human full-length eIF4A (4A), its two single-domain fragments corresponding to the N- and C-terminal domains (AN and AC, respectively), the middle- and C-terminal-domain-linked fragment (GMC) of human eIF4G and its two single-domain fragments corresponding to the middle and C-terminal domains (GM and GC, respectively), and investigated their domain–domain interaction features by surface plasmon resonance (SPR) analysis and isothermal titration calorimetry (ITC). The respective recombinant fragments of human eIF4A and eIF4G used in this work are also shown in Fig. 1.

EXPERIMENTAL PROCEDURES

Plasmid Construction and Expression—The cDNAs of 4A and a GMC mutant (GMC [671–1600] of human eIF4G) were a kind gift from N. Sonenberg (McGill University). The expression plasmid of 4A was constructed from the pET-15b-His vector (Novagene Co.) and that of the GMC gene from the pGEX-6P-GST vector (Amersham Biosciences Co.) in accordance with previously reported methods (*9*, *14*). The full sequences of all the constructs were determined. His-tagged 4A and GST-fused GMC proteins were then expressed in *Escherichia coli* BL21(DE3) (Novagene Co.). The transformed cells were grown in LB broth (Nakarai) containing ampicillin (100 μg/ml) up to an optical density of 0.6 at 600 nm. After the addition of 100 μM and 300 μM IPTG to the cells of His-eIF4A and GST–GMC, respectively, the cells were cultured for 3 h at 30°C (His-4A) and 37°C (GST-GMC). The respective cells were then harvested, suspended in 30 ml of buffer A (50 mM HEPES–NaOH pH 7.4 + 100 mM NaCl) for His-eIF4A or buffer B (50 mM Tris–HCl pH 7.4 + 150 mM NaCl + 1 mM EDTA) for GST–GMC at 0°C and lysed by sonication.

Deletion mutants of 4A (AN and AC) and GMC (GM and GC) were generated on a template of pcDNA-4A and pGEX-6P-1-GMC using PCR with primers containing restriction enzyme sequences of BamHI (3′-primer) for AN, NdeI (5′-primer) and BamHI (3′-primer) for AC, EcoRI (5′-primer) and XhoI (3′-primer) for GM and BamHI (5′-primer) and EcoRI (3′-primer) for GC. The full sequences of all the constructs were determined. These mutant genes were then expressed in *E. coli* BL21 (DE3) in the same manner as the 4A and GMC genes.

Purification of Recombinant Protein—The supernatants of His-tagged 4A, AN and AC cell extracts suspended in buffer A were collected by centrifugation at 18,000 rpm for 90 min and applied to a Chelating Sepharose Fast Flow column (Amersham Biosciences), which was prewashed with buffer A containing 10–50 mM imidazole, and the bound proteins were eluted using buffer A with increasing imidazole concentration (60–90 mM gradient). After the elution, the protein was purified with a Q-HP anion-exchange column using AKTA purifier and with a linear gradient of NaCl using buffers A and B.

On the other hand, the supernatants of the GST-fused GMC, GM and GC cell extracts suspended in buffer B were collected by centrifugation at 18,000 rpm for 90 min and applied to a Glutathione Sepharose 4B affinity column (Amersham Biosciences). After washing the column with buffer B, the bound protein was eluted

with buffer B containing 10 mM reduced glutathione. The protein was then purified with an SP-HP cation-exchange column using AKTA purifier and with a linear gradient of 0–1 M NaCl using buffers A and B. On the other hand, the scission of the GST moiety from its GMC, GM or GC fusion protein was performed using a fusion protein-bound Glutatione Sepharose 4B affinity column using PreScission protease (Amersham Biosciences). The 2 mM protease in buffer B was allowed to react in the column for 14 h at 4°C. After the reaction, the protein was eluted from the column by buffer B and subjected to SP-HP cation-exchange chromatography using SP-HP columns for GM, GC and GMC.

CD Spectroscopy—Each protein solution was adjusted to 10 μM by adding 5 mM HEPES–NaOH buffer (pH 7.4). CD spectra were measured using a JASCO-720 spectrometer in the range of 190–250 nm at a scan speed of 20 nm/min and a sensitivity of 20 mdeg, using a quartz cell of 0.5 mm path length. The temperature dependence of each CD spectrum was investigated in the range of 25–50°C. For each experiment under N_2 gas flow, the measurement was repeated eight times and the measurements obtained were summed. Then, molar ellipticity was determined after normalizing peptide concentration. The same measurement was repeated at least three times using newly prepared samples, to confirm the reproducibility of the results. Data were expressed in terms of mean residue ellipticity [θ] in deg cm^2 $dmol^{-1}$. The contents of α-helix and β-sheet structures were estimated using the CDPro software (CDSSTR) (*28*, *29*).

SPR Analysis—Binding assay was performed using BIAcore X (Biacore, UK). When 4A, AN or AC was used as the ligand molecule, it was immobilized on a CM5 sensor chip by the amine-coupling method or an nitrilotriacetic acid (NTA) sensor chip according to the manufacturer's instructions, where 5 μg/ml protein was reacted in 10 mM sodium acetate buffer (pH 5–6). When the NTA sensor chip was used, it was immobilized by Ni chelation of His-tagged 4A, AN, or AC. In both cases, the sensor chip contained approximately 200–500 RU (resonance unit). GMC, GM or GC was then injected as an analyte molecule over the chip as a function of concentration in the range of 250 nM–10 μM.

On the other hand, when GMC, GM or GC (5 μg/ml) was used as a ligand, it was immobilized on a CM5 sensor chip in the same manner as 4A. For the GST catching method, the anti-GST antigen was immobilized on a CM5 sensor chip, and the GST-fused GMC, GM, or GC was then captured by the GST antibody. In both cases, the sensor chip contained about 1000–1500 RU. 4A, AN or AC as an analyte was injected as a function of concentration. Each cycle consisted of a 40 μl injection of the indicated amount of protein in the BIAcore running buffer (10 mM HEPES–NaOH pH 7.4, 150 mM NaCl, 350 μM EDTA (for CM5) or 50 μM EDTA (for NTA) and 0.005% surfactant P20). The chip was regenerated after each cycle by washing three times with 10–20 μl of regenerating solution (10–30 mM NaOH) or buffer (10 mM glycine–HCl pH 2.2) for the GST catching method. All the measurements were performed at a flow rate of 20 μl/min at 25°C. The obtained sensorgrams were evaluated using the BIA evaluation software package, using which the response from each protein-coated chip with 40 μl of buffer was measured as a reference and was subtracted from the sample response to obtain a sensorgram for the specific interaction.

The kinetic parameters of the association rate k_a, the dissociation rate k_d and the equilibrium dissociation constant KD ($=k_d/k_a$) were estimated from the respective measured sensorgrams in accordance with the obtained SPR profile and curve-fitting pattern: the 1:1 (Langmuir) binding or bivalent binding model for the k_a/k_d-dependent bow-shaped profiles and the steady affinity model (only K_D) for the trapezoid-shaped ones. The respective model fittings yielded reasonable χ^2 values (<10) and distributions of residual plots. The respective kinetic parameters were checked for consistency using local fitting for each analyte concentration.

Isothermal Titration Calorimetry—ITC was performed using a VP-ITC titration calorimetric system (Microcal Inc.). The basic operation for the measurement is as follows: the solution of protein A in the calorimetric cell was titrated with the protein B solution in a titration cell dissolved in the same buffer (20 mM NaH_2PO_4–NaOH pH 7.4 + 100 mM NaCl), where the concentration of A ([A]) was adjusted to be $1 \leq C \leq 1000$ using the relation $C = [A]K_a \times n$ (K_a = association constant of A and B, n = binding ratio of protein A to protein B). Before the measurement, proteins A and B were properly degassed and carefully loaded into the respective cells to avoid bubble formation during stirring, and the heat due to the binding interaction of proteins A and B was determined as the difference between the heat of reaction and the corresponding heat of dilution. In this ITC study, only the combination of protein A = 4A (4–15 μM) in the calorimetric cell and protein B = GMC, GM or GC (50–260 μM) in the titration cell yielded the thermodynamic parameters using the one-site or two-site model. For the 4A–GM and 4A–GMC pairs, the ITC measurement were performed under the absence and presence of equimolar ATP to 4A to investigate the effect of ATP on their interactions, because the helicase activity of eIF4A by eIF4G is stimulated by ATP.

RESULTS

Secondary Structures and Thermal Stabilities of 4A, GMC and their Domains—To determine whether the recombinant proteins have active conformations, their secondary structures were investigated by CD measurements in 5 mM HEPES–NaOH buffer (pH 7.4). Consequently, the high α-helical structure contents were shown for AN, GM, GC and GMC and the distinct β-sheet structures for 4A and AC. These features show that the recombinant proteins take the respective native structures, because these secondary structures clearly reflect the X-ray crystal structures of the N- and C-terminal domains of eIF4A (*24–26*) and the middle and C-terminal domains of eIF4G (*18*, *19*). To investigate the stabilities of these structures, the temperature dependence of their CD spectra was measured and the results of 4A, GMC and their 1:1 mixture are shown in Fig 2A, C and D, respectively. Since the molar ellipticity at 222 nm reflects the secondary structural change,

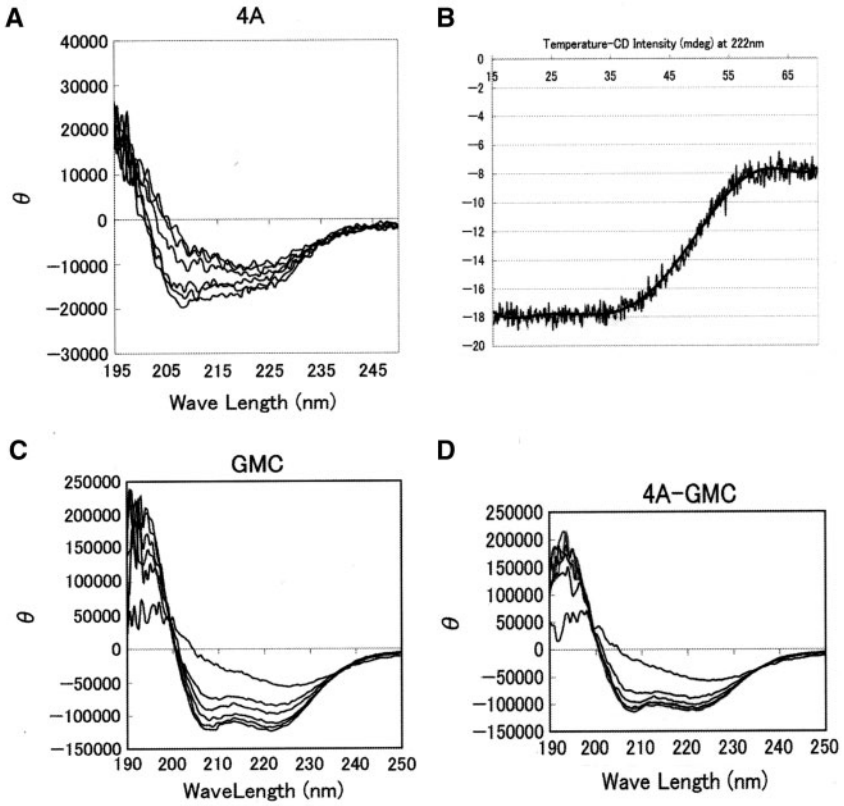

Fig. 2. **Temperature-dependent CD spectral changes of 4A (A), GMC (C) and 4A–GMC (D), and the profile of temperature–molar ellipticity at 222 nm of 4A (B).** The measurements were performed using 2.5 μM samples in 5 mM HEPES buffer (pH 7.4). The temperature of CD spectra of 4A (A), GMC (B) and 1:1 mixture of 4A–GMC (D) corresponds to 15, 25, 37, 42, 47 and 55°C in an increasing [θ] order at 215 nm.

Table 1. **Transition temperatures of secondary structural changes of 4A, GMC and their separated domains.**

4A	44 ± 2°C
AN	47 ± 1°C
AC	46 ± 1°C
GMC	48 ± 1°C
GM	52 ± 1°C
GC	53 ± 1°C
4A + GMC	51 ± 2°C

Transition intermediate temperature was estimated from the profile of temperature—molar ellipticity [θ] at 222 nm.

the molar ellipticity (mdeg) at 222 nm was plotted as a function of temperature to estimate the thermal stability of each structure; an example of 4A is shown in Fig. 2B. The intermediate temperature of the transition curve was used as an index to estimate the thermal stability of each structure and is given in Table 1. It could be said from this table that AN and AC are less stable than GM and GC, and both 4A and GMC are less stable than their component domains, respectively, indicating no collaborative interaction between their domains against thermal deformation. On the other hand, the 1:1 mixture of 4A and GMC resulted in an increased thermal stability by the interaction. The temperature of GMC or 4A alone is considerably increased by the interaction. Because the difference in the temperature of the 4A–GMC complex from that of AN or AC alone is much larger than that of GC or GM alone, this suggests a synergistic effect of the N- and C-terminal domains of 4A on thermal deformation in the interaction with GMC.

SPR Analysis of 4A–GMC and their Domain–Domain Interactions—To estimate the contribution of the respective domains to the 4A–GMC interaction, their binding features were examined by SPR analysis. Because the immobilization of the ligand protein on a CM5 sensor chip by the amine-coupling method causes the random molecular orientation of the protein, this could be the frequent cause of the inaccurate analysis for the interaction of ligand with the analyte protein. Thus, to increase the accuracy of SPR analysis, the interaction was further examined by two different coupling methods, i.e. the NTA Ni-chelation for His-tagged 4A and its two domains (AN and AC) and the GST-antibody binding for GST-fused GMC and its two domains (GM and GC). Thus, the acceptable SPR data were obtained depending on the combination of interaction pairs and on the coupling methods. Essentially, two different SPR profiles were observed for the interaction pairs: one is the usual k_a/k_d-dependent bow-shaped profile and the other is the trapezoid-shaped profile due to the fast association and dissociation rates; their kinetic parameters were

Table 2. **Kinetic parameters of GMC—4A and their domain–domain interactions.**

Ligand	Analyte	Coupling/fitting model	k_a (1/M.s)	k_d (1/s)	K_D (M)
GMC	4A	GST-antibody/bivalent	1.38×10^5	6.02×10^{-2}	$4.36(\pm 0.63) \times 10^{-7}$
4A	GMC	NTA-chip/1:1 langmuir	1.45×10^4	1.53×10^{-3}	$1.05(\pm 0.04) \times 10^{-7}$
GM	4A	GST-antibody/steady affinity			$4.12(\pm 0.39) \times 10^{-7}$
GC	4A	CM5-chip/steady affinity			$4.27(\pm 0.74) \times 10^{-7}$
		GST-antibody/steady affinity			$4.31(\pm 0.39) \times 10^{-7}$
AN	GMC	NTA-chip/1:1 langmuir	8.78×10^3	9.38×10^{-4}	$1.12(\pm 0.18) \times 10^{-7}$

K_D values were derived from k_a and k_d values, which were evaluated from respective sensorgrams using the bivalent or 1:1 Langmuir fitting model. Only K_D values were estimated from the steady affinity model. Standard errors are given in parentheses.

evaluated using the global fitting model for the former profile and the steady affinity model (only *K*D) for the latter profile. Table 2 summarizes the kinetic parameters showing the relevant interaction pairs among all interaction pairs and coupling methods, and some selected SPR profiles are shown in Fig. 3.

(a) Single domain–domain interaction—No acceptable SPR profiles were observed regardless of the coupling method or the combination of ligand and analyte molecules.

(b) Double domain—single or double domain interaction—As for the AC–GMC pair, no notable interaction was observed, regardless of the coupling method or the combination of ligand and analyte molecules. In contrast, the reliable data were obtained for the AN (ligand)–GMC (analyte) pair by the NTA-chip coupling method. The SPR sensorgram was satisfactorily analyzed using the 1:1 (Langmuir) fitting model and estimated to be $K_D = \sim 10^{-7}$ M.

As for the 4A–GM/GC pairs, the acceptable interaction profiles were measured by the CM5-chip (GC) and GST-antibody (GM and GC) coupling methods, when GC/GM was used as the ligand. Characteristically, these pairs showed the trapezoid-shaped profiles due to the fast association and dissociation rates (Fig. 3C and D). The steady affinity model yielded almost the same K_D values for both pairs. Similar K_D values and trapezoid-shaped profiles clearly indicate that the binding modes of 4A with GM and GC are nearly the same but are not very specific to reveal any domain-selective difference. On the other hand, the complex structure of the GM–4A pair was previously determined by NMR [23] and X-ray [24] analyses, and it was clarified that the middle domain of GM binds more strongly to the C-terminal domain of 4A than to the N-terminal one. This is different from the present SPR result, in which no notable binding preference was observed between the N- and C-terminal domains of 4A; this may result from the difference in the observed interaction, i.e. the interaction of analyte with a resin-linked ligand for SPR and free interaction without any binding constraint for NMR or X-ray analysis.

As for the 4A–GMC pair, on the other hand, two kinds of kinetic parameter-dependent binding modes were observed from the SPR profiles, i.e. a 1:1 (Langmuir) model by NTA-chip coupling (Fig. 3A) and a bivalent analyte model by anti-GST-antibody coupling (Fig. 3B). The interaction estimated using the latter model would be almost treated as a 1:1 binding because the second binding affinity ($K_{D2} = \sim 10^{-2}$) is much weaker than the first binding affinity. It is interesting to note that the K_D value is in the same order as those of the GM/GC–4A pairs. This indicates no collaborative effect of the middle and C-terminal domains in GMC on the interaction with 4A. The similar K_D value of the AN–GMC pair also suggests no positive contribution of the 4A C-terminal domain to the interaction with GMC. Because the linker connecting the N- and C-terminal domains of eIF4A could be considerably flexible (*27*), there may be possibility of the simultaneous interactions between the respective domains of 4A and GMC without receiving any restriction from each other.

4A–GMC and Its Domain–domain Interaction as Determined by ITC—ITC was performed to estimate the thermodynamic parameters of the 4A–GMC and its domain–domain interaction pairs. Consequently, the specific binding profiles were mainly observed for the combination of 4A in the calorimetric cell and GMC, GM or GC in the titration cell. The binding parameters are given in Table 3, in which the respective parameters were estimated using the two-site or one-site model, in accordance with the ITC profile pattern. The calorimetric titration profiles of GMC–4A and GM–4A pairs are shown in Fig. 4.

The ITC showed the detectable binding for the GM–AC pair, although this pair showed no specific interaction by the SPR method; this may be also due to the different binding situation, i.e. the ligand molecule-fixed and -unfixed interactions with analyte molecule for the SPR and ITC measurements, respectively. This pair showed two-site bindings with binding ratios of GM/AC = ~0.5 and ~1.5, in which the former binding could be much more specific than the latter one, as shown by their thermodynamic parameters and association constants. This pair showed a positive ΔS, which acts as a driving factor for the complex formation. The complex formation is predominantly promoted by the negative enthalpy change ($-\Delta H$), leading to the negative Gibbs's free energies ($-\Delta G$) of −11.3 and −7.9 kcal/mol. Similarly, two-site binding was also observed for the GM–4A pair. Although the binding parameters are somewhat different from those of the GM–AC pair, the overall binding mode appears to be essentially maintained for the GM–4A pair despite the presence of the 4A N-terminal domain. Because the K_a values at both binding sites are about one-order larger than those of the GM–AC pair, it is obvious that the interaction of 4A with GM is significantly increased by the coexistence of both N- and C-terminal domains of 4A.

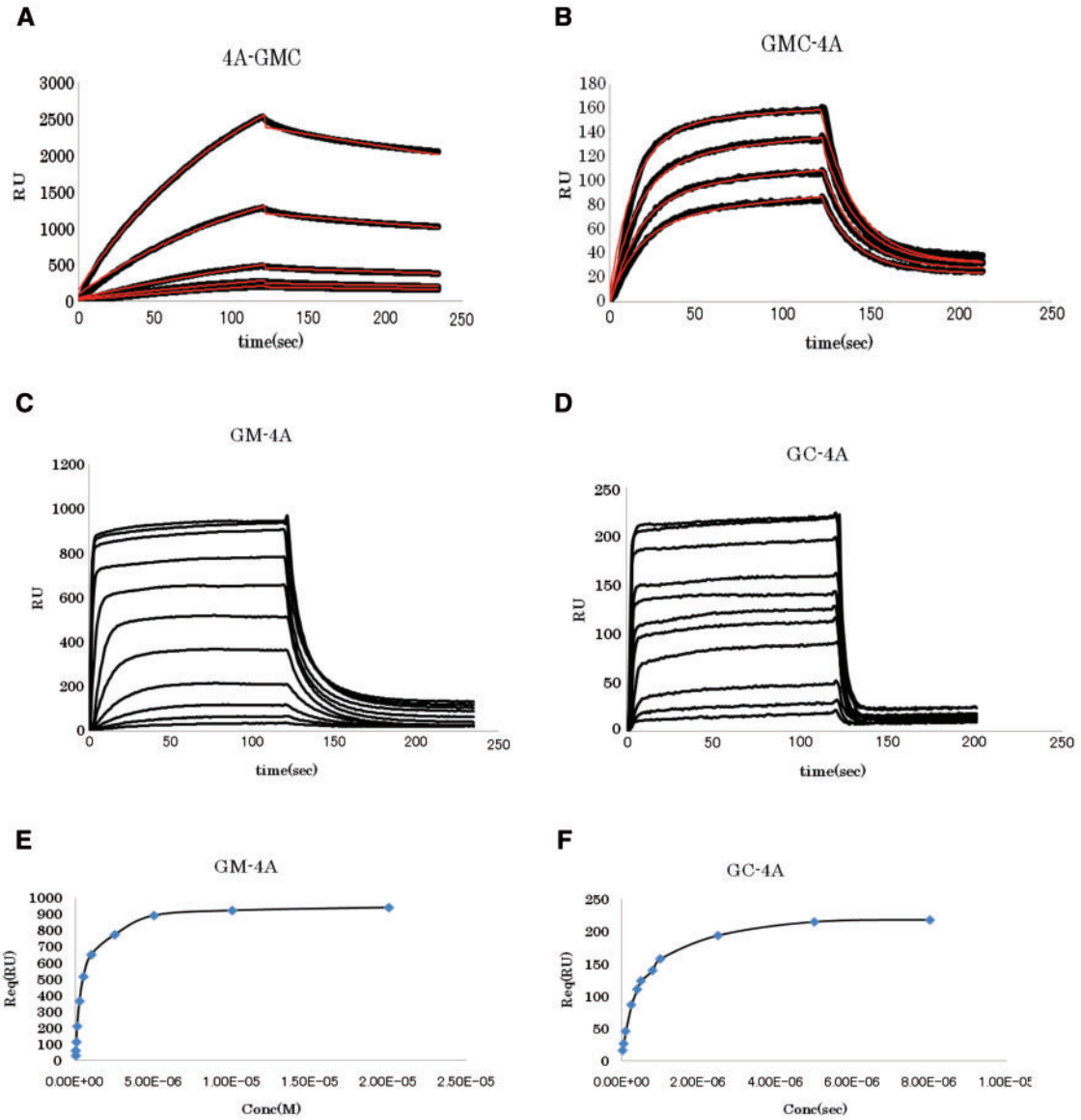

Fig. 3. **SPR profiles of (A) 4A–GMC, (B) GMC–4A, (C) GM–4A and (D) GC–4A pairs.** Respective profiles correspond to the coupling methods of NTA-chip for (A), GST-antibody for (B), (C) and (D). The thin traces (red) in (A) and (B) correspond to the theoretical fitting on the data. Each SPR signal reflects the time response of the addition of analyte: GMC (A) and 4A (B)–(D). The concentration of analyte corresponds to 50, 80, 100, 400 and 500 nM for (A), 25, 40, 50, 80 nM for (B), 10, 25, 50, 100, 250, 500 nM, 1, 2.5, 5, 10 and 20 μM for (C), and 25, 50, 100, 250, 400, 500, 800 nM, 1, 2.5, 5 and 8 μM for (D) in an increasing RU order at 50 s. The right and left parts of each sensorgram at 120 s indicate the phases of binding (injection of analyte) and release (exposure of chip to analyte-free buffer), respectively. The conc. versus RU plots for the GM–4A and GC–4A pairs are shown in (E) and (F), respectively.

In contrast, the ITC of the GC–4A pair showed the one-site binding model of a 1:1 binding, suggesting that GC binds with either the N- or C-terminal domain or simultaneously binds with both domains of 4A with a K_a value of $\sim 10^6$ order. This also indicates that the interaction of the C-terminal domain of 4G with 4A is sufficiently stable to change the binding mode of the GM–4A pair, although the K_a value of the GC–4A pair is considerably smaller than those at the first and second binding sites of the GM–4A pair. This is in contrast with the results of the SPR measurement, in which similar trapezoid-shaped profiles were commonly observed for both pairs.

Similar one-site binding model was also observed for the GMC–4A pair, indicating that the binding mode of the GC–4A pair is essentially maintained. The negative entropy change (ΔS) indicates the interaction on the molecular surface because of the conformational restriction of residues located on the interaction surface. Although this negative value is against the complex formation, the predominant negative enthalpy change (ΔH) leads to a negative Gibbs's free energy ($-\Delta G$) of

Table 3. **Thermodynamic parameters of 4A–GMC and their domain–domain interactions by ITC analysis.**

	−ATP	+ATP
One-site model		
GMC–4A		
n	1.05 (±0.02)	1.09 (±0.02)
K_a (M^{-1})	$3.93\ (\pm0.57) \times 10^6$	$3.84\ (\pm0.67) \times 10^6$
ΔG (cal/mol)	$-8.97\ (\pm0.48) \times 10^3$	$-8.98\ (\pm0.48) \times 10^3$
ΔH (cal/mol)	$-1.79\ (\pm0.05) \times 10^4$	$-1.22\ (\pm0.03) \times 10^4$
$-T\Delta S$ (cal/mol)	8.93×10^3	3.19×10^3
GC–4A		
n	1.03 (±0.02)	
K_a (M^{-1})	$1.16\ (\pm0.15) \times 10^6$	
ΔG (cal/mol)	$-8.27\ (\pm0.03) \times 10^3$	
ΔH (cal/mol)	$-1.27\ (\pm0.03) \times 10^4$	
$-T\Delta S$ (cal/mol)	4.38×10^3	
Two-site model		
GM–4A		
$n1$	0.45 (±0.08)	0.79 (±0.02)
K_a (M^{-1})	$8.29\ (\pm2.97) \times 10^9$	$3.16\ (\pm1.38) \times 10^8$
$\Delta G1$ (cal/mol)	$-1.49\ (\pm0.26) \times 10^4$	$-1.16\ (\pm0.11) \times 10^4$
$\Delta H1$ (cal/mol)	$-1.35\ (\pm0.26) \times 10^4$	$-1.31\ (\pm0.11) \times 10^4$
$-T\Delta S1$ (cal/mol)	-1.42×10^3	1.46×10^3
n_2	1.14 (±0.01)	1.14 (±0.02)
K_a (M^{-1})	$1.30\ (\pm0.22) \times 10^7$	$2.26\ (\pm0.39) \times 10^6$
$\Delta G2$ (cal/mol)	$-8.17\ (\pm0.17) \times 10^3$	$-1.21\ (\pm0.03) \times 10^4$
$\Delta H2$ (cal/mol)	$-8.00\ (\pm0.17) \times 10^3$	$-1.04\ (\pm0.03) \times 10^4$
$-T\Delta S2$ (cal/mol)	-1.71×10^2	-1.70×10^3
GM–AC		
$n1$	0.46 (±0.01)	
K_a (M^{-1})	$2.00\ (\pm\ 1.34) \times 10^8$	
$\Delta G1$ (cal/mol)	$-1.13\ (\pm\ 0.01) \times 10^4$	
$\Delta H1$ (cal/mol)	$-6.80\ (\pm\ 0.18) \times 10^3$	
$-T\Delta S1$ (cal/mol)	-4.53×10^3	
$n2$	1.56 (±0.05)	
K_a (M^{-1})	$6.66\ (\pm0.64) \times 10^5$	
$\Delta G2$ (cal/mol)	$-7.93\ (\pm0.14) \times 10^3$	
$\Delta H2$ (cal/mol)	$-2.54\ (\pm0.14) \times 10^3$	
$-T\Delta S2$ (cal/mol)	-5.39×10^3	

−8.97 kcal/mol for the GMC–4A pair, indicating the exothermic interaction promoted by the enthalpy energy term.

To investigate the effect of ATP on the interactions of 4A with GM and GMC, the ITC measurements were also performed under the presence of equimolar ATP to 4A (Table 3), because the helicase activity of eIF4A is stimulated by ATP. Consequently, it was shown that the association constant of the GM–4A pair is one-order decreased by the presence of ATP, while such a notable change is not observed for the GMC–4A pair. The thermodynamic parameters of the GM–4A pair show that ATP shifts the equal contribution of two sites to the binding with 4A.

DISCUSSION

Despite the 3D structure analyses of the eIF4G middle and C-terminal domains (*18*, *19*), the eIF4A N- and C-terminal domains (*25–27*), and the eIF4G middle domain–eIF4E complex (*23*, *24*), the overall structure of the eIF4A–eIF4G complex has not yet been determined at the atomic level, and the locations of the binding sites on either protein have also remained elusive. Furthermore, the stoichiometry of the interaction is still a subject of controversy (*17*, *20*), and it remains unknown whether eIF4A uses the same or different surfaces for interaction with the two binding domains on eIF4G. Oberer *et al*. (*23*) proposed a binding model of both N- and C-terminal domains of eIF4A to the middle domain of eIF4G by NMR chemical shift mapping and site-directed mutagenesis, and recently, Schutz *et al*. (*24*) have shown the binding structure of eIF4A to the middle domain of eIF4G by X-ray crystallography. However, Korneeva *et al*. (*21*) reported that the N-terminal domain of eIF4A is the primary binding site for the middle domain of eIF4G, and Zakowicz *et al*. (*22*) proposed that the perimeter of the hinge region between the N- and C-terminal domains of eIF4A is the interaction region for eIF4G. Given such ambiguous eIF4A–eIF4G interaction, we systematically investigated possible single, double and mixed domain–domain interactions between both molecules by SPR analysis and ITC.

The SPR analysis provided the following insights: (i) single domain–domain interaction in the 4A–GMC pair is not sufficiently stable to be trapped by the SPR signal, (ii) the interactions of GM/GC with 4A show trapezoid-shaped profiles due to the fast association and dissociation rates, (iii) the 4A–GMC pair almost associates with a 1:1 binding model and (iv) all the interaction pairs showing the SPR-detectable binding take similar K_D values of $\sim10^{-7}$ order despite different coupling method, indicating the lack of concerted domain–domain interactions. On the other hand, the ITC showed the following interaction features: (i) the 4A–GMC and its separated domain–domain interactions are all exothermic and enthalpy-driven reactions and (ii) although the binding of AC/4A to GM proceeds via a two-site binding model, the coexistence of the C-terminal domain (GC or GMC) shifts the binding mode with 4A into a one-site binding model, indicating the marked contribution of the eIF4G C-terminal domain to the interaction with eIF4A.

On the basis of the results of the present SPR analysis and ITC, together with the related reports on possible eIF4A binding regions of eIF4G middle and C-terminal regions (*9*, *18*, *19*, *23*, *24*), we would like to discuss the possible binding between eIF4A and eIF4G. From the SPR results, it could be concluded that the 4A–GMC pair forms a defined and specific binding mode, because it revealed the k_a/k_d-dependent SPR profile, irrespective of the difference in coupling method and the combination of the ligand and analyte molecules. Although the GMC (ligand)–4A (analyte) pair shows two different binding sites, one of them could be negligible because its association constant ($1/K_D$) is extremely smaller than that of the other. Thus, it would be reasonable to consider that the C- and N-terminal domains of eIF4A simultaneously bind to the middle and C-terminal domains of eIF4G, respectively. This is also supported by the finding that the transition temperatures of eIF4A (44°C) and GMC (48°C) are considerably elevated by the 1:1 mixture (51°C) and by the papers (*23*, *24*) that the C-terminal

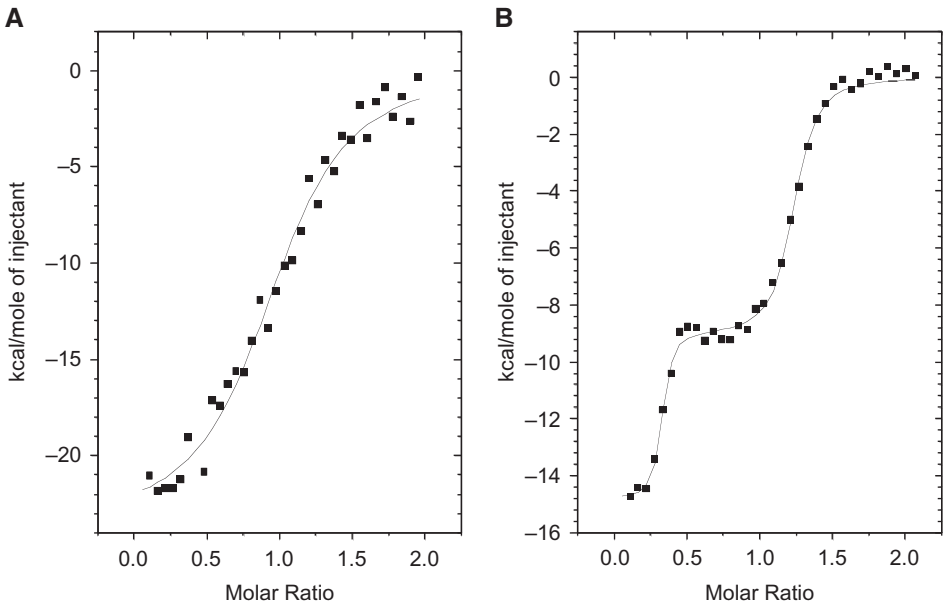

Fig. 4. **Titration calorimetry of (A) GMC–4A and (B) GM–4A pairs in 20 mM NaH_2PO_4-NaOH (pH 7.4) buffer containing 100 mM NaCl.** The panel shows the binding isotherm corresponding to the heat effect associated with the injection of GMC (A) or GM (B) (5 μl per injection of a 60 μM concentration) into the calorimetric cell (1.4 ml) of 4 μM 4A and the best fitted curves (red). The experiments were performed at 25°C.

domain of eIF4A binds to the eIF4G middle domain more preferentially than the N-terminal domain.

On the other hand, the ITC experiment provided another information on the molecular interaction. Among all the possible interaction pairs, only four pairs yielded reliable ITC results. It is noteworthy that AC/4A interacts with GM via the two-site binding model, and that the interaction profile of 4A with GC/GMC showed a one-site binding model. This clearly indicates that when the middle domain (GM) of eIF4G interacts with the C-terminal (AC) or both domains (4A) of eIF4A, GM could accommodate both domains (4A) with nearly the same binding mode as the binding with AC without any significant structural change of the middle domain. This ITC profile of the GM–4A pair appears to reflect the structural feature clarified by NMR (*24*) and X-ray (*25*) analyses. The C-terminal domain of 4A would bind to one of the two binding sites in GM (n1), as judged from the thermodynamic parameters and association constants. Then, the second binding site (n2) would be occupied by the 4A N-terminal domain with a 1:1 binding. Generally, it is considerable that the interaction of GM with the 4A C-terminal domain proceeds via the 1:1 binding ratio. However, the ITC showed a molar ratio of n1 = ~1/2. Although we could not explain the molar ratio reasonably, it might have resulted from the conformational change of 4A following the binding to GM, because it has been proposed that the binding of the 4A C-terminal domain to GM causes the conformational change of 4A, but not that of GM, so as to enable the interaction of the N-terminal domain with GM (*24*).

In contrast, the ITC profile of the GMC–4A pair showed the one-site binding model. This clearly shows that the interaction mode of the eIF4A–eIF4G pair could not be modeled by that of the GM–4A pair. The kinetic parameters of the GMC–4A pair suggest the preferential binding of 4A to the C-terminal domain of GMC. Another notable difference between the GMC–4A and GM–4A pairs could be observed for their entropy changes (Table 3). Generally, a negative entropy change is observed when a molecule forms a complex with another via a molecular surface binding region, because conformational freedom is generally restricted by complex formation. This is the case of the former pair. However, the latter pair showed a positive entropy change, which might be due to the enhanced solvation entropy (hydrophobic effect), combined with a reduced loss of conformational entropy of 4A upon binding to the structurally rigid moiety of GM, such as a binding pocket.

On the basis of the ITC and SPR results, a possible binding model of eIF4A and eIF4G molecules is proposed in Fig. 5, in which the red-colored solid ellipse represents a binding region via molecular surface interaction between AC and GC and dominates the binding feature between 4A and GMC, whereas the dotted ellipse represents the binding region, which is not predominant, but important for the binding of 4A with GMC. On the other hand, the red-colored dots represent the GM binding pockets which characterize the binding of 4A, when 4A binds with GM. The previous results showed the importance of GM for the biological function of 4A, because the middle domain of eIF4G could bind both the N-terminal and C-terminal domain of eIF4A and is sufficient for enhancing the eIF4A helicase activity (*23*, *24*) and for the recruitment of mRNA and scanning (*9*). This suggests that the solid dots on GM are the essential region for revealing the helicase activity of eIF4A, and two ellipses on GC are the interaction regions that serve as regulating or maturing/completing the biological

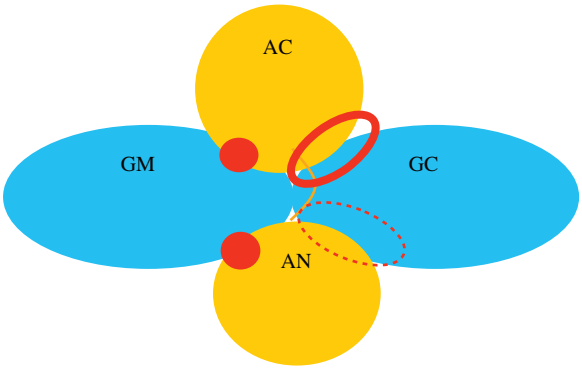

Fig. 5. **Schematic binding model of eIF4A (yellow)–eIF4G (blue) molecules.** The red-color filled circles represent the eIF4A-binding pockets of middle domain of eIF4G in the absence of C-terminal domain. The red-colored solid and dotted ellipses represent the binding regions *via* molecular surface interactions of eIF4A C- and N-terminal domains with the C-terminal domain of eIF4G, respectively.

function of eIF4A. However, the ITC results of 4A–GM and 4A–GMC pairs in the presence of ATP clearly showed the importance of C-terminal domain of eIF4G for the ATP-simulated helicase activity of eIF4A, because the binding mode of the latter pair is little influenced by the contribution of ATP, while that of the former pair is considerably deformed. This means that the overall fixation of the eIF4A structure by the two domain-straddled binding with eIF4G is advantageous for the effective catalytic function of eIF4A. The present result also clarified that eIF4A uses the different surfaces for interaction with the two binding domains on eIF4G.

In conclusion, the present study showed that not only the middle region but also the C-terminal region of eIF4G plays an important role in the intact biological manifestation of eIF4A, in other words, the whole structural analysis of the GMC–4A complex is necessary to understand the enhancement of the eIF4A helicase activity by eIF4G.

FUNDING

Grant-in-Aid for High Technology Research from the Ministry of Education, Culture, Sports, Science and Technology, Japan.

CONFLICT OF INTEREST

None declared.

REFERENCES

1. Sonenberg, N. and Dever, T.E. (2003) Eukaryotic translation initiation factors and regulators. *Curr. Opin. Struct. Biol.* **13**, 56–63
2. Kapp, L.D. and Lorsch, J.R. (2004) The molecular mechanics of eukaryotic translation. *Annu. Rev. Biochem.* **73**, 657–704
3. Marintchev, A. and Wagner, G. (2005) Translation initiation: structures, mechanisms and evolution. *Q. Rev. Biophys.* **37**, 1–88
4. Gingras, A.-C., Raught, B., and Sonnenberg, N. (1999) eIF4 initiation factors: effectors of mRNA recruitment to ribosomes and regulators of translation. *Annu. Rev. Biochem.* **69**, 913–963
5. Linder, P. (2003) Yeast RNA helicases of the DEAD-box family involved in translation initiation. *Biol. Cell* **95**, 157–167
6. Sengoku, T., Nureki, O., Nakamura, A., Kobayashi, S., and Yokoyama, S. (2006) Structural basis for RNA unwinding by the DEAD-box protein *Drosophila Vasa*. *Cell* **125**, 287–300
7. Hentze, M.W. (1997) eIF4G: a multipurpose ribosome adapter? *Science* **254**, 500–501
8. Morley, S.J., Curtis, P.S., and Pain, V.M. (1997) eIF4G: translation's mystery factor begins to yield its secrets. *RNA* **3**, 1085–1104
9. Morino, S., Imataka, H., Svitkin, Y.V., Pestova, T.V., and Sonenberg, N. (2000) Eukaryotic translation initiation 4E (eIF4E) binding site and the middle one-third of eIF4GI constitute the core domain for cap-dependent translation, and the C-terminal one-third functions as a modulatory region. *Mol. Cell. Biol.* **20**, 468–477
10. Mader, S., Lee, H., Pause, A., and Sonenberg, N. (1995) The translation initiation factor eIF-4E binds to a common motif shared by the translational factor eIF-4G and the translational repressors 4E-binding proteins. *Mol. Cell. Biol.* **20**, 6019–6029
11. Tarun, S.Z. Jr. and Sachs, A.B. (1996) Association of the yeast poly(A) tail binding protein with translation initiation factor eIF-4G. *EMBO J.* **15**, 7168–7177
12. Imataka, H., Gradi, A., and Sonenberg, N. (1998) A newly identified N-terminal amino acid sequence of human eIF4G binds poly(A)-binding protein and functions in poly(A)-dependent translation. *EMBO J.* **17**, 7480–7489
13. Lamphear, B.J., Kirchweger, R., Skem, T., and Rhoads, R.E. (1995) Mapping of functional domains in eukaryotic protein synthesis initiation factor 4G (eIF4E) with picornaviral proteases. Implications for cap-dependent and cap-independent translational initiation. *J. Biol. Chem.* **270**, 21975–21983
14. Imataka, H. and Sonenberg, N. (1997) Human eukaryotic translation initiation factor 4G (eIF4G) possesses two separate and independent binding sites for eIF4A. *Mol. Cell. Biol.* **17**, 6940–6947
15. Pyronnet, S., Imataka, H., Gingras, A.-C., Fukunaga, R., Hunter, T., and Sonenberg, N. (1999) Human eukaryotic translation initiation factor 4G (eIF4G) recruits Mnk1 to phosphorylate eIF4E. *EMBO J.* **18**, 270–279
16. Dominguez, D., Altmann, M., Benz, J., Baumann, U., and Trachsel, H. (1999) Interaction of translation initiation factor eIF4G with eIF4A in the yeast *Saccharomyces cerevisiae*. *J. Biol. Chem.* **274**, 26720–26726
17. Korneeva, N.L., Lamphear, B.J., Colby Hennigan, F.L., Merrick, W.C., and Rhoads, R.E. (2001) Characterization of the two eIF4A-binding sites on human eIF4G-1. *J. Biol. Chem.* **276**, 2872–2879
18. Marcotrigiano, J., Lomakin, I.B., Sonenberg, N., Pestova, T.V., Hellen, C.U.T., and Burley, S.K. (2001) A conserved HEAT domain within eIF4G directs assembly of the translation initiation machinery. *Mol. Cell* **7**, 193–203
19. Bellsolell, L., Cho-Park, P.F., Poulin, F., Sonenberg, N., and Burley, S.K. (2006) Two structurally atypical HEAT domains in the C-terminal portion of human eIF4G support binding to eIF4A and Mnk1. *Structure* **14**, 913–923
20. Li, W., Belsham, G.J., and Proud, C.G. (2001) Eukaryotic initiation factors 4A [eIF4A] and 4G [eIF4G] mutually interact in a 1:1 ratio *in vivo*. *J. Biol. Chem.* **276**, 29111–29115
21. Korneeva, N.L., First, E.A., Benoit, C.A., and Rhoads, R.E. (2005) Interaction between the NH_2-terminal domain of eIF4E and the central domain of eIF4G modulates RNS-stimulated ATPase activity. *J. Biol. Chem.* **280**, 1872–1881
22. Zakowicz, H., Yang, H.-S., Stark, C., Wlodawer, A., Laronde-Leblanc, N., and Colburn, N.H. (2005) Mutational analysis of the DEAD-box RNA helicase eIF4AII

characterizes its interaction with transformation suppressor Pdcd4 and eIF4GI. *RNA* **11**, 261–274
23. Oberer, M., Marintchev, A., and Wagner, G. (2005) Structural basis for the enhancement of eIF4A helicase activity by eIF4G. *Genes Dev.* **19**, 2212–2223
24. Schutz, P., Bumann, M., Oberholzer, A.E., Bieniossek, C., Trachsel, H., Altmann, M., and Baumann, U. (2008) Crystal structure of the yeast eIF4A–eIF4G complex: an RNA-helicase controlled by protein–protein interactions. *Proc. Natl Acad. Sci. U.S.A* **105**, 9564–9569
25. Benz, J., Trachsel, H., and Baumann, U. (1999) Crystal structure of the ATPase domain of translation initiation factor 4A from *Saccharomyces cerevisiae*—the prototype of the DEAD box protein family. *Structure* **7**, 671–679
26. Johnson, E.R. and McKay, D.B. (1999) Crystallographic structure of the amino terminal domain of yeast initiation factor 4A, a representative DEAD-box RNA helicase. *RNA* **5**, 1526–1534
27. Caruthers, J.M., Johnson, E.R., and McKay, D.B. (2000) Crystal structure of yeast initiation factor 4A, a DEAD-box RNA helicase. *Proc. Natl Acad. Sci. U.S.A* **97**, 13080–13085
28. Sreerama, N. and Woody, R.W. (2000) Estimation of protein secondary structure from circular dichroism spectra: comparison of CONTIN, SELCON, and CDSSTR methods with an expanded reference set. *Anal. Biochem.* **287**, 252–260
29. Sreerama, N., Venyaminov, S.Y., and Woody, R.W. (2001) Analysis of protein circular dichroism spectra based on the tertiary structure classification. *Anal. Biochem.* **299**, 271–274